Results in Physics 8 (2018) 537–544

Contents lists available at ScienceDirect

Results in Physics

journal homepage: www.journals.elsevier.com/results-in-physics

Thermal Marangoni convection in two-phase flow of dusty Casson fluid

B. Mahanthesh [a,*], B.J. Gireesha [b]

[a] Department of Mathematics, Christ University, Bangalore 560029, India
[b] Department of Studies and Research in Mathematics, Kuvempu University, Shankaraghatta, 577451 Shimoga, Karnataka, India

ARTICLE INFO

Article history:
Received 7 December 2017
Received in revised form 22 December 2017
Accepted 24 December 2017
Available online 29 December 2017

Keywords:
Marangoni convection
Dusty fluid
Casson fluid
Two-phase flow
Runge-Kutta-Fehlberg method

ABSTRACT

This paper deals with the thermal Marangoni convection effects in magneto-Casson liquid flow through suspension of dust particles. The transpiration cooling aspect is accounted. The surface tension is assumed to be fluctuating linearly with temperature. The fluid and dust particle's temperature of the interface is chosen as a quadratic function of interface arc length. The governing problem is modelled by conservation laws of mass, momentum and energy for fluid and dust particle phase. Stretching transformation technique is utilized to form ordinary differential equations from the partial differential equations. Later, the numerical solutions based on Runge-Kutta-Fehlberg method are established. The momentum and heat transport distributions are focused on the outcome of distinct governing parameters. The results of Nusselt number is also presented and discussed. It is established that the heat transfer rate is higher in the case of dusty non-Newtonian fluid than dusty Newtonian fluid. The rate of heat transfer can be enhanced by suspending dust particles in a base liquid.

Introduction

Fluid flow embedded with identical immiscible inert solid particles is known as a two-phase fluid system. The theory of two/multi-phase fluids dreadfully accommodates in the understanding of the physical phenomena of engineering circumstances such as the lunar ash flows, cement production, steel manufacturing industry, combustion, wastewater treatment, powder technology, dust in gas cooling systems and atmospheric fallout. Evidently, two-phase investigations are precious in modelling and understanding of the physical phenomena. Even such studies are mathematically challenging. To cite some of the past and recent studies on the flow and heat transfer analysis, Saffman [1] was the first to develop expressions for viscous liquid flow with the insertion of immiscible inert solid particles. Singleton [2] initiated to scrutinize the impact of dust particles suspension in a liquid under boundary layer assumptions. Ezzat et al. [3] examined the free convection in dusty-liquid transition through a porous medium. Sivaraj and Rushi [4] reported analytic solutions for viscoelastic liquid flows with variable mass diffusion in the irregular channel through a suspension of dust particles. Numerical simulations are provided by Siddique et al. [5] for two-phase particulate suspension flow on vertical surface. They were treated governed equations via implicit two-point finite difference method. Siddique et al. [6] examined the contaminated air and water flow with the impact of radiation past a cone wavy frustum. Hossain et al. [7] studied the role of a small discrepancy in surface temperature and free stream velocity in dusty liquid with mixed convection. How the linear deformation of the wall affects the dusty-liquid material 3D flow was investigated in the work of Mohaghegh and Rahimi [8]. Sandeep and his research group [9,10] explored the impact of suspending dust particles in nano liquid over deformable sheet under steady and unsteady flow situations. Very recently, Mustafa [11] presented the analytic solutions for two-phase dusty liquid flow and heat model over deforming isothermal surfaces. Gireesha and co-workers [12–15]) contributed to an advancement of the two-phase dusty liquid topic under distinct aspects.

Some of working fluids such as molten plastics, polymeric liquids, artificial fibers, blood, foodstuffs, slurries and synovial fluid exhibit non-Newtonian fluid characteristics. Such fluids exhibit shear-stress-strain relationships which are significantly distinct from the Newtonian model. Most of the non-Newtonian models involve some form of modification to the momentum equations. In the category of non-Newtonian fluids, the Casson liquid has distinct features. It has significant applications in polymer processing industries and biomechanics. The Casson liquid model is sometimes stated to fit rheological data better than the general viscoplastic model for many materials. In this context, many authors ([16–24] and references therein) are studied the heat transfer flow of Casson liquid with distinct physical aspects.

* Corresponding author.
E-mail address: mahanthesh.b@christuniversity.in (B. Mahanthesh).

https://doi.org/10.1016/j.rinp.2017.12.066
2211-3797/© 2017 Published by Elsevier B.V.

Nomenclature

(x, y)	Cartesian coordinates (m)
t_0, T_0	constants
l	dust particle mass concentration
t_∞	fluid ambient temperature (K)
q_w	fluid phase heat flux
t	fluid temperature (K)
h	Local heat transfer coefficient
Nu_x	local Nusselt number
B_0	magnetic field strength
M	magnetic parameter
m	mass and of dust particles
T_∞	particle ambient temperature (K)
T	particle temperature (K)
Pr	Prandtl number
r_p	radius of dust particles
L	reference length (m)
C_p	specific heat of the dust particles ($m^2s^{-2}k^{-1}$)
C	specific heat of the fluid ($m^2s^{-2}k^{-1}$)
S	suction/injection parameter
k	thermal conductivity (W/mK)
(u, v)	velocity fields of fluid (m/s)
(U, V)	velocity fields of particle phase (m/s)
p_y	yield stress

Greek symbols

β	Casson fluid parameter
π_c	critical value of product of the component of the rate of strain tensor with itself
μ	dynamic viscosity (Kg/ms)
σ^*	electrical conductivity (S/m)
ρ	fluid density (Kg/m^3)
ν	kinematic viscosity (m^2/s)
β_v	momentum dust parameter
τ_v	momentum relaxation time
ρ_p	particle density (Kg/m^3)
μ_B	plastic dynamic viscosity
γ_T	rate of change of surface tension with respect to fluid temperature
γ	specific heat ratio
$\psi(x, y)$	streams functions of fluid
$\Psi(x, y)$	streams functions of particle phase
v_0	suction/injection velocity
σ	surface tension
σ_0	surface tension at the interface
β_T	thermal dust parameter
τ_T	thermal relaxation time

Superscripts

$'$	derivative with respect to ξ

Besides, the mechanism of Marangoni convective boundary layer transport has been the focus of widespread research during the last two decades. The Marangoni boundary layer is the dissipative layer, which takes place along the liquid-liquid or liquid-gas interfaces. Due to the surface temperature/concentration gradient created Marangoni flow finds relevance in aerospace engineering, crystal growth, combustion, chemical reaction process, coating, silicon melt, nuclear reactors and thin liquid films (see [39] and references therein). Pop et al. [25] examined the features of thermosolutal boundary layer Marangoni convection phenomena. Al-Mudhaf and Chamkha [26] discussed the aspects of heat generation or absorption on thermosolutal Marangoni convection on a planar surface. They utilized the stretching transformations scheme for the solution purpose. Magyari and Chamkha [27] revealed the impact of Marangoni convection under high Reynolds number flow assumptions. They reported the exact solutions for the problem. In the work of Zheng et al. [28], the Marangoni convection caused by temperature gradient on a liquid-vapour surface is analytically analyzed. Again Zheng et al. [29] explored the Marangoni mixed convective phenomena by accounting power law liquids and temperature distribution of linear variety. Further, impacts of magnetism and chemical reaction on Marangoni mixed convection were examined in the work of Zhang et al. [30]. Marangoni magneto-convective flow case was scrutinized by Ibrahim [32] by accounting the impacts of Joule, radiative and dissipative heating. Sreenivasulu et al. [33] studied magnetism consequence on Marangoni thermosolutal convection in viscous liquid with Joule and viscous heating. Latest researches concerning on Marangoni boundary layer convective heat and mass transport mechanism under various aspects can be found in [34–39].

It is clear from aforesaid literature survey that, the Marangoni convective phenomena in the flow of dusty-Casson-liquid is not yet investigated. Thus, our objective of this research is to scrutinize the features of Marangoni convection in dusty Casson-Liquid. Transpiration cooling and magnetism are also accounted. The surface tension is assumed to be fluctuating linearly with temperature. Numeric solutions are developed for the governed problem through shooting and Runge-Kutta-Fehlberg scheme [12–15].

Formulation

In a rectangular coordinate system, x and y are taken along the plate and normal to it correspondingly, and flow confined at $y \geqslant 0$ (see Fig. 1). A steady Marangoni two-phase boundary layer flow of particulate non-Newtonian Casson fluid is considered. Flow is two dimensional and laminar on permeable plate under the influence of homogeneous magnetic field of magnitude B_0. The interface temperature of both fluid and particle is assumed to be quadratic functions of the distance x along the interface. The surface tension (Marangoni) aspect acts as a boundary condition on the governing flow field equations. The surface tension σ is supposed to depend on linear fluctuation with temperature as $\sigma = \sigma_0[1 - \gamma_T(t - t_\infty)]$, here σ_0 is the surface tension at the interface and $\gamma_T = -\frac{1}{\sigma_0}\frac{\partial\sigma}{\partial t}$ rate of change of surface tension with respect to fluid temperature. Let $\psi(x, y)$ and $\Psi(x, y)$ are streams functions

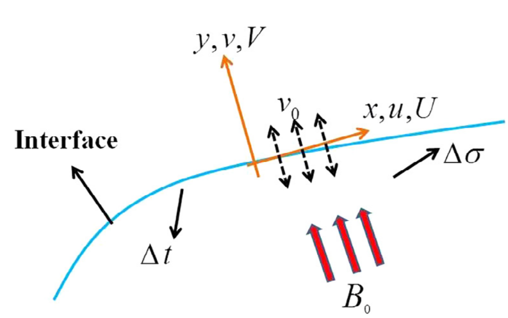

Fig. 1. The Physical geometry of the problem.

of fluid and particle phase such that $u=\frac{\partial\psi}{\partial y}, U=\frac{\partial\Psi}{\partial y}, v=-\frac{\partial\psi}{\partial x}$ and $V=-\frac{\partial\Psi}{\partial x}$. In terms of stream functions, the governing equations can be written as (see [2,11,37]);

Fluid phase:

$$\frac{\partial^2\psi}{\partial y\partial x}-\frac{\partial^2\psi}{\partial x\partial y}=0, \tag{1}$$

$$\rho\left(\frac{\partial\psi}{\partial y}\frac{\partial^2\psi}{\partial y\partial x}-\frac{\partial\psi}{\partial x}\frac{\partial^2\psi}{\partial y^2}\right)=\mu\left(1+\frac{1}{\beta}\right)\frac{\partial^3\psi}{\partial y^3}+\frac{\rho_p}{\tau_v}\left(\frac{\partial\Psi}{\partial y}-\frac{\partial\psi}{\partial y}\right)-\sigma^* B_0^2\frac{\partial\psi}{\partial y} \tag{2}$$

$$\rho C\left(\frac{\partial\psi}{\partial y}\frac{\partial t}{\partial x}-\frac{\partial\psi}{\partial x}\frac{\partial t}{\partial y}\right)=k\frac{\partial^2 t}{\partial y^2}+\frac{\rho_{pC_p}}{\tau_T}(T-t) \tag{3}$$

Particle phase:

$$\frac{\partial^2\Psi}{\partial y\partial x}-\frac{\partial^2\Psi}{\partial x\partial y}=0, \tag{4}$$

$$\rho_p\left(\frac{\partial\Psi}{\partial y}\frac{\partial^2\Psi}{\partial y\partial x}-\frac{\partial\Psi}{\partial x}\frac{\partial^2\Psi}{\partial y^2}\right)=-\frac{\rho_p}{\tau_v}\left(\frac{\partial\Psi}{\partial y}-\frac{\partial\psi}{\partial y}\right) \tag{5}$$

$$\rho_p C_p(\frac{\partial\psi}{\partial y}\frac{\partial T}{\partial x}-\frac{\partial\psi}{\partial x}\frac{\partial T}{\partial y})=-\frac{\rho_{pC_p}}{\tau_T}(T-t) \tag{6}$$

Along with the boundary conditions (see [11,37]);

$$\mu\left(1+\frac{1}{\beta}\right)\frac{\partial^2\psi}{\partial y^2}\bigg|_{y=0}=\frac{\partial\sigma}{\partial x}\bigg|_{y=0},\quad -\frac{\partial\psi}{\partial x}\bigg|_{y=0}=v_0,$$
$$t(x,0)=t_\infty+t_0X^2,\quad X=\frac{x}{L}, \tag{7}$$

$$\frac{\partial\psi}{\partial y}\bigg|_{y\to\infty}=0,\quad \frac{\partial\Psi}{\partial y}\bigg|_{y\to\infty}=0,\quad \frac{\partial\psi}{\partial x}\bigg|_{y\to\infty}=\frac{\partial\Psi}{\partial x}\bigg|_{y\to\infty},$$
$$t(x,\infty)=t_\infty,\quad T(x,\infty)=T_\infty \tag{8}$$

here (u,v) and (U,V) are velocity fields of fluid and parti ρ_p cle phase respectively, t – fluid temperature, T – particle temperature, $\beta=\frac{\mu_B\sqrt{2\pi_c}}{p_y}$ – Casson fluid parameter, μ_B – plastic dynamic viscosity, p_y – yield stress, π_c – critical value of product of the component of the rate of strain tensor with itself, ρ – fluid density, ρ_p – particle density, μ – dynamic viscosity, v – kinematic viscosity, σ^* – electrical conductivity, B_0 – magnetic field strength, k – thermal conductivity, $\tau_v=m/6\pi\mu r_p$ is momentum relaxation time, $\tau_T=mC_p/4\pi r_p$ thermal relaxation time, m and r_p are the mass and radius of dust particles, C and C_p specific heat of the fluid and dust particles, t_0, T_0 – constants, t_∞ and T_∞ – fluid and particle ambient temperature, L – reference length and v_0 – suction/injection velocity.

Introducing the following stretching transformations [27]

$$\psi(x,y)=vXf(\xi),\quad \Psi(x,y)=vXg(\xi),\quad \xi=y/L,$$

$$t(x,y)=t_\infty+t_0X^2\theta(\xi),\quad T(x,y)=T_\infty+T_0X^2\Theta(\xi) \tag{9}$$

into the partial boundary value problem (Eqs. (1)–(8)), one can have following ordinary differential system;

$$f'''(\xi)+f'''(\xi)f(\xi)-f'(\xi)^2+l\beta_v[g'(\xi)-f'(\xi)]-Mf'(\xi)=0, \tag{10}$$

$$g''(\xi)g(\xi)-g'(\xi)^2+\beta_v[f'(\xi)-g'(\xi)]=0. \tag{11}$$

$$\frac{1}{Pr}\theta''(\xi)+\theta'(\xi)f(\xi)-2f'(\xi)\theta(\xi)+l\beta_T\gamma(\Theta(\xi)-\theta(\xi))=0, \tag{12}$$

$$\Theta'(\xi)g(\xi)-g'(\xi)\Theta(\xi)-\beta_T[\Theta(\xi)-\theta(\xi)]=0 \tag{13}$$

with boundary conditions

$$f''(\xi)|_{\xi=0}=-2\left(1+\frac{1}{\beta}\right)^{-1},\quad f(\xi)|_{\xi=0}=S,\quad \theta(\xi)|_{\xi=0}=1,$$
$$f'(\xi)|_{\xi\to\infty}=0,\quad g'(\xi)|_{\xi\to\infty}=0,\quad g(\xi)|_{\xi\to\infty}=f(\xi)|_{\xi\to\infty}, \tag{14}$$
$$\theta(\xi)|_{\xi\to\infty}=0,\quad \Theta(\xi)|_{\xi\to\infty}=0,$$

here dust particle mass concentration, momentum dust parameter, magnetic parameter, suction/injection parameter, Prandtl number, specific heat ratio, thermal dust parameter are correspondingly defined as

$$l=\frac{\rho_p}{\rho},\quad \beta_v=\frac{L^2}{\tau_v v},\quad M=\frac{\sigma B_0^2L^2}{\rho v},\quad S=-\frac{v_0L}{v},\quad Pr=\frac{\mu C}{k},\quad \gamma=\frac{C_p}{C},\quad \beta_T=\frac{L^2}{\tau_T v}$$

The fluid phase heat flux can be written as

$$q_w=-k\frac{\partial t}{\partial y}\bigg|_{y=0}, \tag{15}$$

Local heat transfer coefficient h is given by;

$$h=\frac{q_w}{t_0X^2}, \tag{16}$$

The local Nusselt number, which physical quantity of interest of our study is given by;

$$Nu_x=\frac{hx}{k}=-\left(\frac{x}{L}\right)\theta'(\xi)\bigg|_{\xi=0}. \tag{17}$$

Solution procedure

The nonlinear boundary value expressions (10)–(13) are converted to set of single order initial value problem before solving them by RKF-45 method. Now use the following set of variables;

$$f=y_1,\quad f'=y_2,\quad f''=y_3,\quad f'''=y_3',\quad g=y_4,\quad g'=y_5,\quad g''=y_5',$$
$$\theta=y_6,\quad \theta'=y_7,\quad \Theta=y_8,\quad \Theta=y_8'. \tag{18}$$

In view of (18), Eqs. (10)–(13) takes following form

$$y_1'=y_2,\quad y_2'=y_3,\quad y_3'=y_2^2+My_2+l\beta_v(y_2-y_5)-y_1y_3,$$
$$y_4'=y_5,\quad y_5'=y_4^{-1}[y_5^2+\beta_v(y_5-y_2)],\quad y_6'=y_7,$$
$$y_7'=\Pr[2y_2y_6+l\beta_T\gamma(y_6-y_8)-y_1y_7],\quad y_8'=y_4^{-1}[y_5y_8+\beta_T(y_8-y_6)] \tag{19}$$

respective boundary conditions are

$$y_1(0)=S,\quad y_2(0)=m_1,\quad y_3(0)=-2,\quad y_4(0)=m_2,$$
$$y_5(0)=m_3,\quad y_6(0)=1,\quad y_7(0)=m_4,\quad y_8(0)=m_5 \tag{20}$$

here m_1 to m_5 are unknowns and they are determined by shooting method. More details of the employed method and validations can see in our papers [12–15]. To assess the accuracy of our employed method, a comparative study is presented (see Tables 1 and 2). Comparison results reveal an outstanding agreement.

Table 1
Comparison of skin friction coefficient $(1+\frac{1}{\beta})f''(0)$ values with that of Hayat et al. [16] when $S=l=0$, $M=0.5$ and the Marangoni condition $f''(\xi)|_{\xi=0}=-2(1+\frac{1}{\beta})^{-1}$ is replaced by $f'(\xi)|_{\xi=0}=1$.

β	Hayat et al. [16] Homotopy Analysis Method	Present Results (RKF-45 method)
0.8	1.67705	1.67712
1.4	1.46385	1.46386
2.0	1.36931	1.36931
3.0	1.29099	1.29099

Table 2
Comparison of $f''(0)$ values with that of Tufail et al. [17] and Cortel et al. [40] when $S=l=0$, $\beta\to\infty$ and the Marangoni condition $f''(\xi)|_{\xi=0}=-2(1+\frac{1}{\beta})^{-1}$ is replaced by $f'(\xi)|_{\xi=0}=1$.

M	Tufail et al. [17] (Kummer's function)	Cortel et al. [40] (Runge–Kutta algorithm)	Present Results (RKF-45 method)
0.0	1.00000	1.00000	1.00000
0.5	1.22475	1.22475	1.22475
1.0	1.41421	1.41421	1.41421
1.5	1.58114	1.58114	1.58114
2.0	1.73205	1.73205	1.73205
2.5	1.87083	–	1.87083
3.0	2.00000	–	2.00000

Interpretation of the results

The influence of Marangoni convection on two-phase dusty non-Newtonian fluid over a planar plate is studied for the first time. The main focus of this section is to explore the physical behaviour of fluid velocity ($f'(\xi)$), dust velocity ($g'(\xi)$), fluid temperature ($\theta(\xi)$) and dust temperature profiles ($\Theta(\xi)$) for the impact of dust particle mass concentration (l), momentum dust parameter (β_v), thermal dust parameter (β_T), magnetic parameter (M) and suction/injection parameter (S). To this end Figs. 2–10 are plotted. Further, numerical values of Nusselt number is presented in Table 3. It is key to note that for $l=0$, the flow governs Marangoni convection for carrier phase only (i.e., without dust particles). Also the projected problem illustrates two different flow problems under following cases:

i. $\beta\to\infty$stand for the Newtonian dusty fluid flow problem,
ii. Finite value of β stand for the non-Newtonian dusty Casson fluid flow problem.

The curves of $f(\xi), g(\xi), f'(\xi), g'(\xi), \theta(\xi)$ and $\Theta(\xi)$ versus similarity variable ξ are captured in Fig. 2 for DCF (dusty Casson fluid), DF (dusty fluid) and CF (Casson fluid) cases. It is seen that fluid phase primary velocity profile $f(\xi)$ is higher for DF case than DCF and CF cases in order. This trend is qualitatively same for $g(\xi)$, but quantitatively higher than $f(\xi)$. Next we see that $f'(\xi), g'(\xi), \theta(\xi)$ and $\Theta(\xi)$ fields are decreasing as ξ grows. All these profiles are asymptotically approached and satisfy the far field boundary condition. This led more assurance about the correctness of the reported solution. Here we see that, the velocity profile of both carrier and particle phase ($f'(\xi)$ and $g'(\xi)$) is higher for CF case than DCF and DF cases. Besides, CF case thermal fields ($\theta(\xi)$ and $\Theta(\xi)$) are larger than DF and DCF cases.

Impact of l on $f'(\xi)$ and $g'(\xi)$ is sketched in Fig. 3. An increment in l reduce the flow in both phases. The carrier fluid phase and particle phase are coupled in the course of drag force and phenomena of heat exchange. An increase in dust particle volume fraction boosts drag force within the fluid. Consequently, the velocity profiles are reduced. Also, the thickness of velocity boundary layer is smaller for particulate fluid than that of clean fluid. Fig. 4 exhibits the impact of l on $\theta(\xi)$ and $\Theta(\xi)$. As mass concentartion of dust increases more β_T dust particles gain the heat energy from the carrier fluid. Thus, temperature of the carrier fluid declines, relatively particle phase thermal field also decreased. (See Fig. 4). Further, the thickness of energy boundary layer is large for clean fluid when we compared with particulate fluid. Fig. 5 reveals the plots for β_v on $f'(\xi)$ and $g'(\xi)$. Here the $f'(\xi)$ component decreases and $g'(\xi)$ component significantly increases for larger β_v. The plots for on $\theta(\xi)$ and $\Theta(\xi)$ can be found in Fig. 6. Clearly, $\theta(\xi)$ decreases and $\Theta(\xi)$ increases by increasing β_T. Such behaviour is obvious since the basefluid loses the kinetic and thermal energy via intermingle with dust particles. Therefore, carrier fluid velocity/temperature fields decreased as we strengthen the momentum/thermal dust parameter. This phenomenon holds in contrary for particle phase velocity/temperature.

Fig. 7 represents the $f'(\xi)$ and $g'(\xi)$ curves for M. Here both $f'(\xi)$ and $g'(\xi)$ reduces as M is increased. This outcome is expected because the larger M strengthens Lorentz force in the flow region. This force has propensity to diminish velocity of both phases. Impact of M on $\theta(\xi)$ and $\Theta(\xi)$ profiles is qualitatively opposite as compared to $f'(\xi)$ and $g'(\xi)$ profiles (see Fig. 8). Fig. 9 addresses the consequences of S on $f'(\xi)$ and $g'(\xi)$. Here negative values of S indicates the injection aspect and positive values represents suction aspect. Fig. 9 reveals that, the influence of suction and injection are contradictory. The outcome of $\theta(\xi)$ and $\Theta(\xi)$ is qualitatively same as compared to $f'(\xi)$ and $g'(\xi)$ profiles with respect to the influence of S. (see Fig. 10). Further we observe from Figs. 2–10 that, the magnitude dusty Casson fluid velocity and momentum boundary layer thickness is higher as compared to

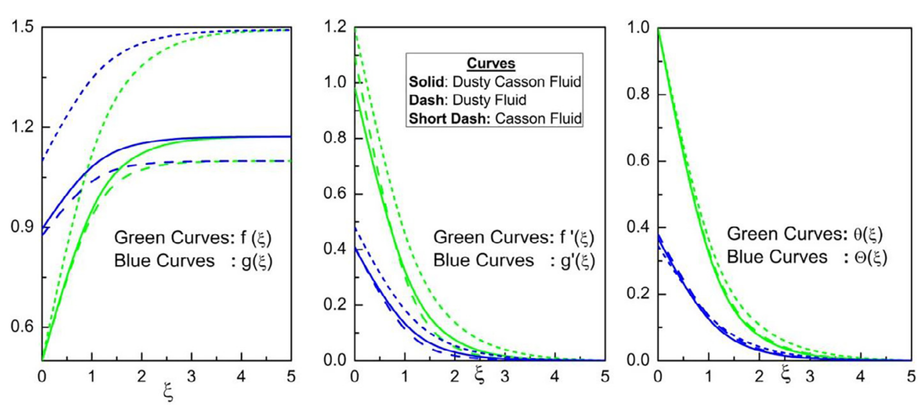

Fig. 2. Profiles of $f(\xi), g(\xi), f'(\xi), g'(\xi), \theta(\xi)$ and $\Theta(\xi)$ versus similarity variable ξ.

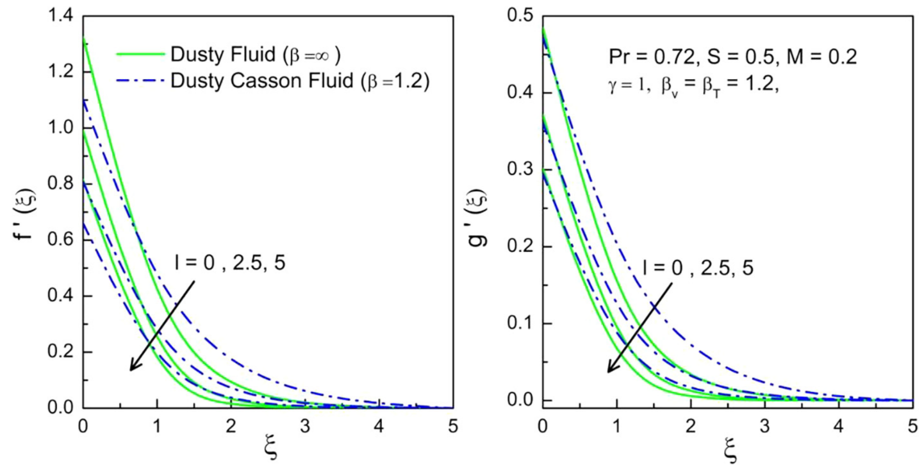

Fig. 3. Impact of l on $f'(\xi)$ and$g'(\xi)$.

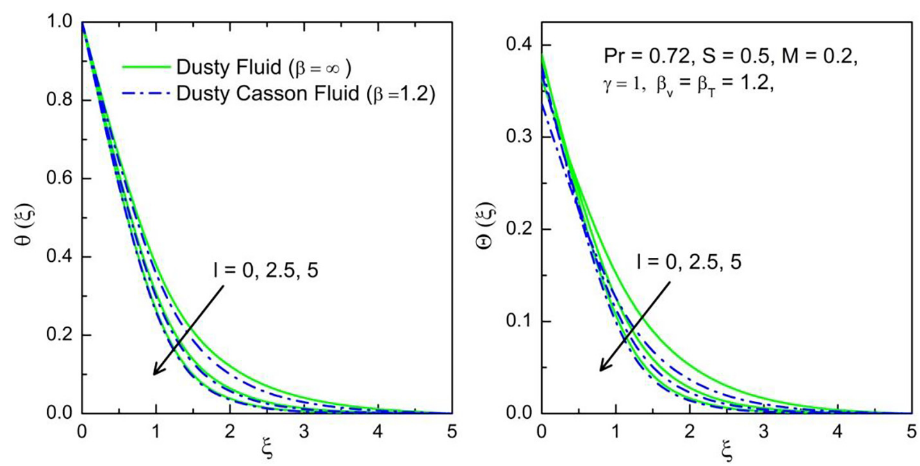

Fig. 4. Impact of l on $\theta(\xi)$ and $\Theta(\xi)$.

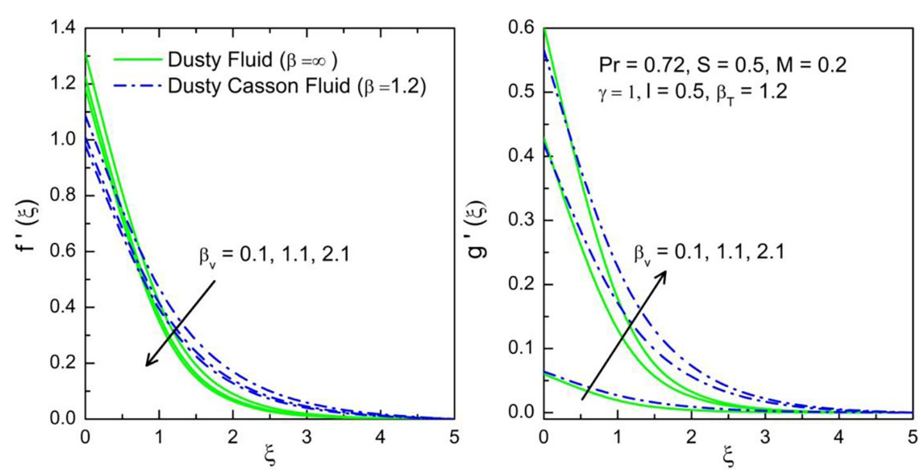

Fig. 5. Impact of β_v on $f'(\xi)$ and $g'(\xi)$.

dusty fluid velocity case. The thermal boundary layer is thicker for dustyfluid than that of dusty Casson fluid. However, the characteristics of flow fields of dustyfluid and dusty Casson fluid are qualitatively same.

Finally, Table 3 presented to scrutinize the impact of l, β_T, Pr, S and M on Nu_x for DCF and DF cases. Table 1 shows decay of Nu_x via applied magnetic field. But, the Nu_x is incremented as the values of l, β_T, Pr and S are enhanced. The Nu_x is augmented due to adding dust particles into the carrier fluid, i.e., Nu_x is larger for $l \neq 0$ in comparison with $l = 0$. Further, rate of heat transfer at the surface for DCF case is larger as we compared with DF case.

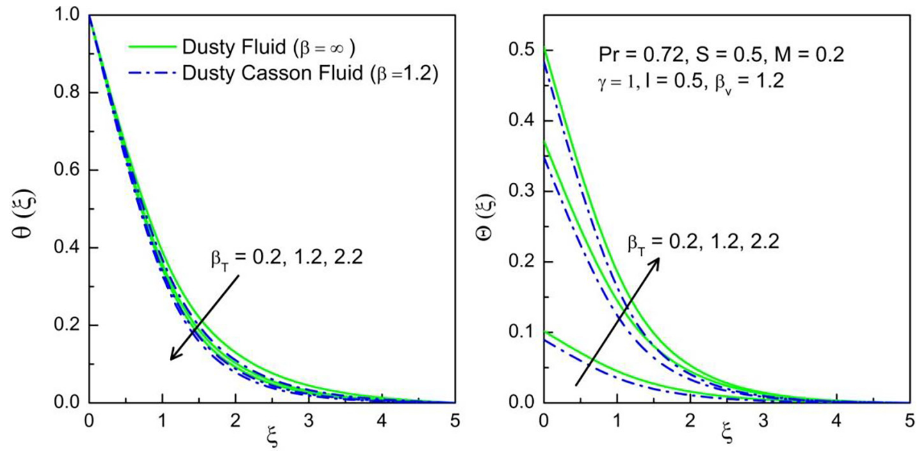

Fig. 6. Impact of β_T on $\theta(\xi)$ and $\Theta(\xi)$.

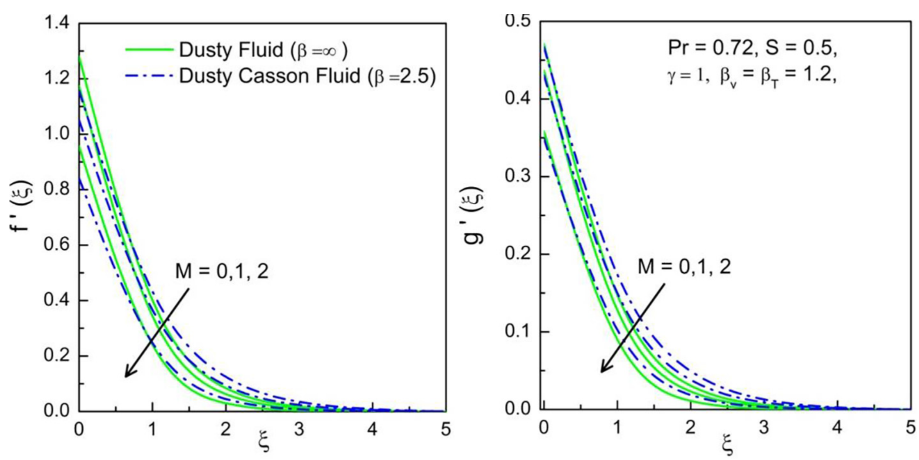

Fig. 7. Impact of M on $f'(\xi)$ and $g'(\xi)$.

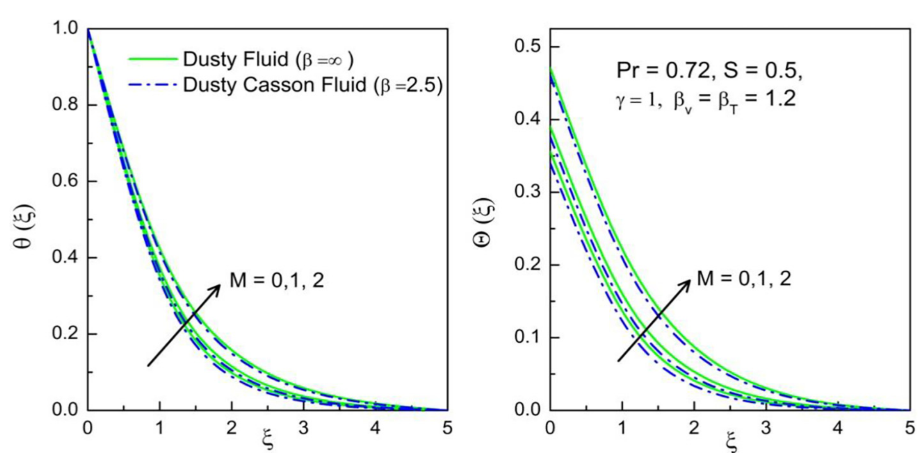

Fig. 8. Impact of M on $\theta(\xi)$ and $\Theta(\xi)$.

Concluding remarks

The major outcomes are:

- The magnetic field is used to accelerate the thermal field. But the velocity of both phases diminished.
- The momentum and thermal layer decreased via dust particle concentration parameter. Thus, it can be used as a key aspect to control the two-phase flow fields.
- The carrier fluid velocity/temperature reduced via momentum/thermal dust parameter. But, this trend is converse to particle phase fields.
- Impact of suction and injection are contrary.

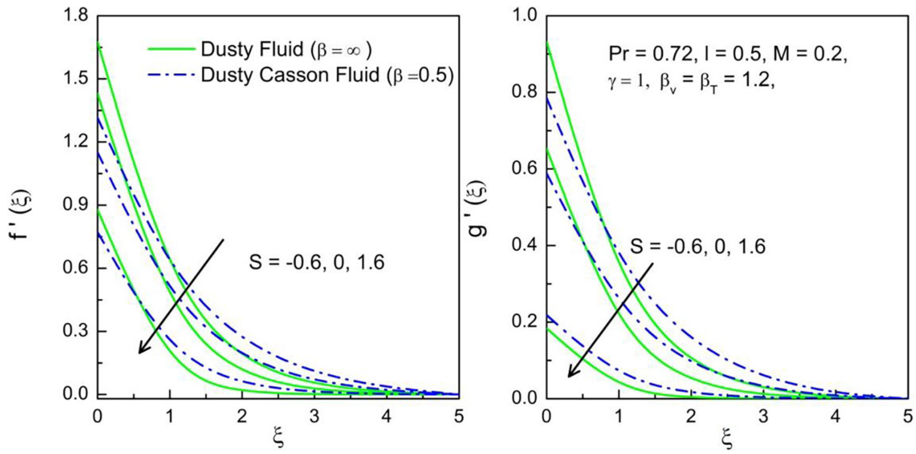

Fig. 9. Impact of S on $f'(\xi)$ and$g'(\xi)$.

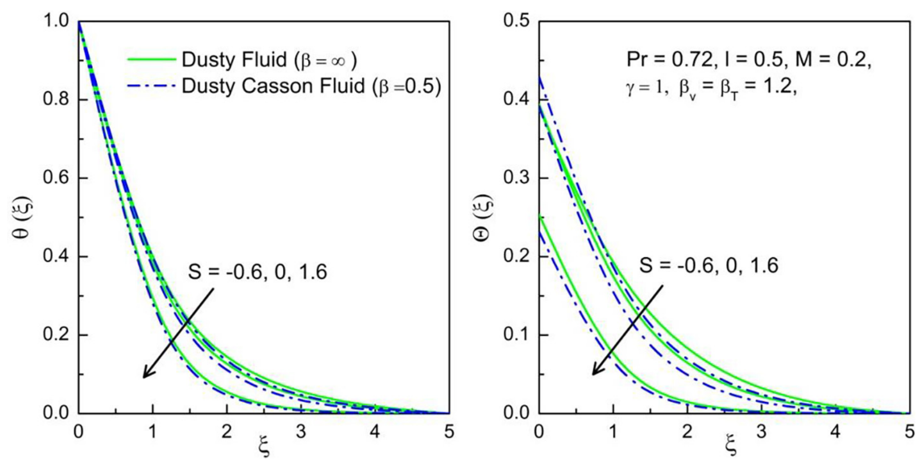

Fig. 10. Impact of S on $\theta(\xi)$ and $\Theta(\xi)$.

Table 3
Results of Nu_x versus l, β_T, Pr, S and M for dusty Casson fluid and Dustyfluid.

l	β_T	Pr		M	S Nu_x	
					Dusty Casson fluid $\beta = 2.5$	Dustyfluid $\beta \to \infty$
0	1.2	0.72	0.5	0.2	1.395197	1.393731
1					1.526992	1.524676
2					1.663032	1.658961
0.5	**0.5**				1.397931	1.396860
	1.5				1.478718	1.476576
	2.5				1.524101	1.520243
	2.5	**0.72**			1.524101	1.520243
		3			3.981078	4.049326
		6.2			6.523570	6.650555
		3	**−0.5**		2.601160	2.759009
			0		3.207889	3.320542
			0.5		3.981078	4.049326
			−0.5	**0.2**	2.601160	2.759009
				0.3	2.558940	2.718172
				0.4	2.517739	2.678242

- The rate of heat transfer can be enhanced by suspending dust particles in the base fluid.
- The Nu_x decreased via applied magnetic field. But, the Nu_x is incremented as the values of l, β_T, Pr and S are enhanced.
- The Nu_x is larger for dusty non-Newtonian fluid than dusty Newtonian fluid.

References

[1] Saffman PG. The stability of laminar flow of a dusty gas. J Fluid Mech 1962;13:120–8.
[2] Singleton RE. Fluid mechanics of gas-solid particle flow in boundary layers [Ph. D. Thesis]. California Institute of Technology; 1964.
[3] Ezzat MA, El-Bary AA, Morsey MM. Space approach to the hydro-magnetic flow of a dusty fluid through a porous medium. Comput Math Appl 2010;59:2868–79.
[4] Sivaraj R, Kumar BR. Unsteady MHD dusty viscoelastic fluid Couette flow in an irregular channel with varying mass diffusion. Int J Heat Mass Transfer 2012;55:3076–89.
[5] Siddiqa S, Hossain MA, Saha SC. Two-phase natural convection flow of a dusty fluid. Int J Numer Methods Heat Fluid Flow 2015;25:1542–56.
[6] Siddiqa S, Begum N, Hossain MA, Massarotti N. Influence of thermal radiation on contaminated air and water flow past a vertical wavy frustum of a cone. Int Commun Heat Mass Transfer 2016;76:63–8.
[7] Hossain MA, Roy NC, Siddiqa S. Unsteady mixed convection dusty fluid flow past a vertical wedge due to small fluctuation in free stream and surface temperature. Appl Math Comput 2017;293:480–92.
[8] Mohaghegh MR, Rahimi AB. Three-dimensional stagnation point flow and heat transfer of a dusty fluid toward a stretching sheet. J Heat Transfer 2016;138:112001.
[9] Sandeep N, Sulochana C. MHD flow of dusty nanofluid over a stretching surface with volume fraction of dust particles. Ain Shams Eng J 2016;7(2):709–16.
[10] Sandeep N, Sulochana C, Kumar BR. Unsteady MHD radiative flow and heat transfer of a dusty nanofluid over an exponentially stretching surface. Eng Sci Technol Int J 2016;19(1):227–40.
[11] Turkyilmazoglu M. Magnetohydrodynamic two-phase dusty fluid flow and heat model over deforming isothermal surfaces. Phys Fluids 2017;29:013302.
[12] Gireesha BJ, Mahanthesh B, Manjunatha PT, Gorla RSR. Numerical solution for hydromagnetic boundary layer flow and heat transfer past a stretching surface embedded in non-Darcy porous medium with fluid-particle suspension. J Nigerian Math Soc 2015;34(3):267–85.
[13] Gireesha BJ, Mahanthesh B, Gorla RSR, Manjunatha PT. Thermal radiation and Hall effects on boundary layer flow past a non-isothermal stretching surface embedded in porous medium with non-uniform heat source/sink and fluid-particle suspension. Heat Mass Transfer 2016;52(4):897–911.
[14] Gireesha BJ, Mahanthesh B, Gorla RSR, Krupalakshmi KL. Mixed convection two-phase flow of Maxwell fluid under the influence of non-linear thermal radiation, non-uniform heat source/sink and fluid-particle suspension. Ain Shams Eng. Journal 2016. https://doi.org/10.1016/j.asej.2016.04.020.
[15] Krupa Lakshmi KL, Gireesha BJ, Gorla RSR, Mahanthesh B. Effects of diffusion-thermo and thermo-diffusion on two-phase boundary layer flow past a stretching sheet with fluid-particle suspension and chemical reaction: A numerical study. J Nigerian Math Soc 2016;35(1):66–81.
[16] Hayat T, Shehzad SA, Alsaedi A. Soret and Dufour effects on magnetohydrodynamic (MHD) flow of Casson fluid. Appl Math and Mech 2012;33:1–12.
[17] Tufail MN, Butt AS, Ali A. Heat source/sink effects on non-Newtonian MHD fluid flow and heat transfer over a permeable stretching surface: Lie group analysis, Indian. J. Phys. 2013;88:75–82.
[18] Ibrahim W, Makinde OD. Magnetohydrodynamic stagnation point flow and heat transfer of Casson nanofluid past a stretching sheet with slip and convective boundary condition. J Aerosp Eng 2016;29(2).
[19] Benazir AJ, Sivaraj R, Makinde OD. Unsteady magnetohydrodynamic Casson fluid flow over a vertical cone and flat plate with non-uniform heat source/sink. Int J Eng Res Africa 2016;21:69–83.
[20] Shashikumar NS, Archana M, Prasannakumara BC, Gireesha BJ, Makinde OD. Effects of nonlinear thermal radiation and second order slip on Casson nanofluid flow between parallel plates. Defect Diffus Forum 2017;377:84–94.
[21] Gireesha BJ, Archana M, Prasannakumara BC, Gorla RSR, Makinde OD. MHD three dimensional double diffusive flow of Casson nanofluid with buoyancy forces and nonlinear thermal radiation over a stretching surface. Int J Numer Methods Heat Fluid Flow 2017;27(12):2858–78.
[22] Gireesha BJ, Sampath Kumar PB, Mahanthesh B, Shehzad SA, Rauf A. Nonlinear 3D flow of Casson-Carreau fluids with homogeneous–heterogeneous reactions: A comparative study. Results Phys 2017;7:2762–70.
[23] Rehman KU, Malik AA, Malik MY, Sandeep N, Saba NU. Numerical study of double stratification in Casson fluid flow in the presence of mixed convection and chemical reaction. Results Phys 2017;7:2997–3006.
[24] Kumaran G, Sandeep N, Ali ME. Computational analysis of magnetohydrodynamic Casson and Maxwell flows over a stretching sheet with cross diffusion. Results Phys 2017;7:147–55.
[25] Pop I, Postelnicu A, Grosan T. Thermosolutal Marangoni forced convection boundarylayers. Meccanica 2001;36:555–71.
[26] Al-Mudhaf A, Chamkha AJ. Similarity solutions for MHD thermosolutal Marangoni convection over a flat surface in the presence of heat generation or absorption effects. Heat Mass Transfer 2005;42(2):112–21.
[27] Magyari E, Chamkha AJ. Exact analytical solutions for thermosolutal Marangoni convection in the presence of heat and mass generation or consumption. Heat Mass Transfer 2007;43:965–74.
[28] Zheng L, Xinxin Z, Gao Y. Analytical solution for Marangoni convection over a liquid-vapor surface due to an imposed temperature gradient. Math Comput Model 2008;48:1787–95.
[29] Zhang Y, Liancun Z, Wang X, Song G. Analysis of Marangoni convection of non-Newtonian power law fluids with linear temperature distribution. Therm Sci 2011;15:45–52.
[30] Zhang Y, Liancun Z. Analysis of MHD thermosolutal Marangoni convection with the heat generation and a first-order chemical reaction. Chem Eng Sci 2012;69:449–55.
[32] Sreenivasulu P, Reddy NB, Reddy MG. Effects of radiation on MHD thermosolutal Marangoni convection boundary layer flow with Joule heating and viscous dissipation. Int J Appl Math Mech 2013;9:47–65.
[33] Arifin NM, Nazar R, Pop I. Similarity solution of Marangoni convection boundary layer flow over a flat surface in a nanofluid. J Appl Math 2013;2013.
[34] Lin Y, Zheng L, Zhang X. Radiation effects on Marangoni convection flow and heat transfer in pseudo-plastic non-Newtonian nanofluids with variable thermal conductivity. Int J Heat Mass Transfer 2014;77:708–16.
[35] Lin Y, Zheng L. Marangoni boundary layer flow and heat transfer of copper-water nanofluid over a porous medium disk. AIP Adv 2015;5(10):107225.
[36] Mahdy A, Sameh EA. Thermosolutal Marangoni boundary layer magnetohydrodynamic flow with the Soret and Dufour effects past a vertical flat plate. Eng Sci Technol Int J 2015;18:24–31.
[37] Hayat T, Uzma S, Anum S, Alsaedi A, Asghar S. Marangoni mixed convection flow with Joule heating and nonlinear radiation. AIP Adv 2015;5(7):077140.
[38] Lin Y, Li B, Zheng L, Chen G. Particle shape and radiation effects on Marangoni boundary layer flow and heat transfer of copper-water nanofluid driven by an exponential temperature. Powder Technol 2016;301:379–86.
[39] Hayat T, Khan MI, Farooq M, Alsaedi A, Yasmeen T. Impact of Marangoni convection in the flow of carbon-water nanofluid with thermal radiation. Int J Heat Mass Transfer 2017;106:810–5.
[40] Cortell R. A note on magnetohydrodynamic flow of a power-law fluid over a stretching sheet. Appl Math Comput 2005;168:557–66.